Local mechanisms of cohesive soil erosion

F. Brunier-Coulin, P. Cuéllar & P. Philippe
IRSTEA, UR RECOVER, 3275 route de Cézanne
CS 40061, 13182 Aix-en-Provence Cedex 5, France

ABSTRACT: The present study provides an experimental contribution to a better understanding of erosion mechanisms, based on a parametric analysis with different model materials. Such model soils allow for a controlled variation of physical properties, as well as the particle size and shape, and even the cohesion and bonding strength which can be quantified by specific mechanical testing devices. In parallel, the soil's resistance against erosion can also be somehow quantified by means of experimental procedures such as the JET test (Hanson and Cook 2004). The goal of the investigations presented here is to determine the soil's mechanical properties having a strong impact on the erosion resistance, and thus being required in an efficient erosion model. The useful case where the model material is also transparent enables, with adapted optical equipment, the time-space monitoring of single soil particles during erosion and thus a local analysis of erosion and soil's detachment. Experimentally, this condition is achieved by using an oil mixture as eroding fluid and a model soil made out of glass beads possibly bonded with a very viscous liquid, all phases having approximately the same refractive index. Coupling then this refractive index matching technique with the planar laser-induced fluorescence, as already used by Philippe & Badiane (2013), makes it possible to observe the mechanisms by which the fluid flow removes single particles from the cohesive material.

1 INTRODUCTION

Soil erosion is a natural phenomenon characterised by the detachment and transport of elementary soil particles under the action of air or water. Erosion by a fluid flow is a physical process resulting from the response of a soil to hydrodynamic stress. This stress depends on the kinetics of the fluid, generally turbulent, at the interface of a cohesive soil.

The phenomenon by which a fluid flow may cause the dislodgement of primary soil particles is a key problem for many fields, as in the coastal engineering for the prediction of estuary and river bed evolution (Parchure & Mehta 1985), (Dufois et al. 2014), or in the civil engineering for the assessment of the stability and durability of earthen hydraulic structures. In the latter case, Foster et al. (2000) identify that 90% of embankment dams failures are due to erosion. Around 50% of these failures are caused by surface erosion due to overflowing, and the other 50% by an internal erosion due to infiltrations. In France there are in average approximately one failure of dams and one failure of protection dikes per year. In order to enhance the safety of earthen hydraulic structures, it is important to comprehend better the elementary mechanisms involved during erosion processes at the surface of a soil sample. In particular, the local phenomena of water erosion of a cohesive material composed of sand, mud and/or clay exposed to a fluid flow are still poorly understood and their current modelling can be improved.

The erosion discussed in this paper concerns the interaction between an initially static solid phase, composed by the soil, and a water flow. The water flow causes pressure and velocity gradients resulting into hydrodynamic stresses τ_e at the soil surface. The erosion process can be described by a critical stress τ_c above which, particles constituting the soil begin to be dislodged by the water flow. Above this threshold, the soil will be eroded at a rate which in principle seems to depend on the excess stress $\tau_e - \tau_c$. This rate can be quantified by a coefficient of erosion k. In this fashion, Parteniades (1965) proposed the following relation of the erosion rate, ϵ_r proportionally to the excess shear stress:

$$\epsilon_r = \begin{cases} k_d(\tau_e - \tau_c) & \text{if } \tau_e > \tau_c \\ 0 & \text{if not} \end{cases} \quad (1)$$

Where ϵ_r is the eroded volume of soil per unit of surface and time $[m.s^{-1}]$, k_d is the mass coefficient of erosion in $[m^2.s.kg^{-1}]$ and τ_c the critical stress.

This simple linear empirical law has a good correlation with many experimental data, and is used in most studies on soil's resistance to erosion (Ariathurai and Arulanandan 1978), (Hanson and Cook 2004), (Benahmed and Bonelli 2012). However, several alternative erosion laws exist as a power law (VanRijn 1984) or an exponential law (Parchure and Mehta 1985). Also note that these laws are based on a mean hydrodynamic shear stress, related more or less empirically to the fluid velocity and pressure gradient, both of them parameters which are averaged in time and space. But, since the fluid flow is generally turbulent, these parameters are fluctuating, and such fluctuation can be used in a statistical expression of the shear stress based on a Gaussian distribution of the velocity, as proposed by VanProoijen & Winterwerp (2010). Spatial variability of the fluid flow can also be accounted for by a similar statistical approach as described by Béguin et al. (2013).

Both parameters k_d and τ_c are *a priori* inherent to the material. They can be estimated empirically by adjusting the previous empirical law with specific erosion tests. Such erosion tests consist in generating a controlled hydrodynamic stress applied at the interface of a soil sample to measure the erosion rate. However, it is difficult to obtain a clear correlation between these parameters and other common soil properties. The goal of the present study is to perform a parametric study aiming to identify the local mechanisms by which a fluid flow can dislodge soil's particles. The challenge is to identify the most relevant parameters in the resistance to erosion, to be compared to the erosion parameters and thereafter to be implemented in erosion laws.

Here, we will present two cohesive model materials, one with solid bondings and one with viscous bondings. With the first material ($M1$), specific tests were performed to relate its mechanical behaviour with its resistance to erosion while changing some of the material characteristics. Next, we will discuss the impact of viscous bondings on the erosion process with the second material ($M2$). This artificial soil permits the spatio-temporal monitoring of the erosion process under the influence of an impinging jet flow.

2 MODEL MATERIALS

Soils are composed of elementary particles where the size may define a possible cohesion between the grains. This cohesion provides some resistance to the material deformation and come from capillary forces or atomic, chemical or electric attractive forces. It can take place either directly between two grains (adhesion), or through bonds constituted by the finest fraction of the soil (cohesion).

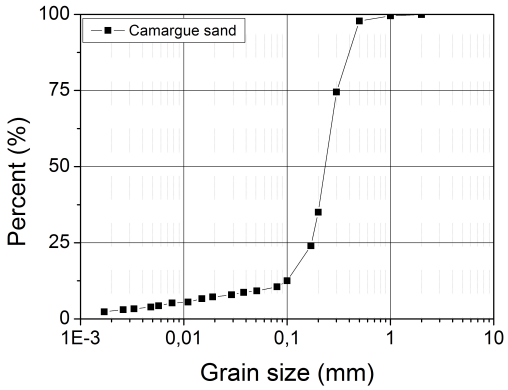

Figure 1: Size distribution of the Camargue sand (France) used for the model soil with solid bonds ($M1$): $D_{50} = 240\mu m$

The parametric study presented in this paper makes use of several model materials for which it is possible to change specifically some of their characteristics. In this section we briefly describe the two different model materials used to investigate erosion mechanisms and related soil's resistance.

2.1 *MATERIAL $M1$: SOLID BONDINGS*

The first material is a natural sand bonded with a small quantity of paraffin. Figure 1 presents the size distribution of the sand from Camargue (France), used as a granular medium for this first material. This sand is mixed with different volumes of paraffin at $100°$C to create capillary liquid paraffin bridges since paraffin fusion temperature is $62°$C. After cooling at ambient temperature, these bridges became solid bondings and we obtain a brittle material. The paraffin content controls the size of the solid bridges between particles, and thus their related inter-granular cohesive forces. With adapted hydrodynamic solicitations and mechanical tests to measure these contact forces, it is possible to analyse the impact of this cohesion on the resistance to erosion as will be discussed in Section 3.

2.2 *MATERIAL $M2$: VISCOUS BONDINGS*

The second material has been developed to be completely transparent and to make possible a visualisation inside the material. For this purpose, the refractive indexes of the granular medium and the cohesive matrix are accurately matched.

This model soil is made of a granular phase composed of borosilicate glass beads which have a refractive index $n = 1.472$. The cohesive bondings are created with a very viscous fluid, namely a yield-stress fluid, which has almost the same refractive index. As a first choice, we used a transparent synthetic clay, the Carbopol gel, as described for instance by Luu et al. (2015). A second choice for a cohesive matrix was the Ucon™ Oil, a very viscous liquid ($\mu_{UO} = 4.10^4 cP$) which has also approximately the same refractive index. The quantity of Ucon™ Oil can control the size of the viscous bondings, which will then

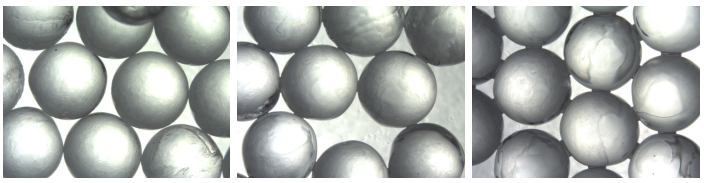

Figure 2: Model soil with viscous cohesion ($M2$): Borosilicate glass beads of 3mm diameters with 0.1, 0.5 and 1% in mass of Ucon^{TM} Oil. The oil content controls the size of the viscous bondings

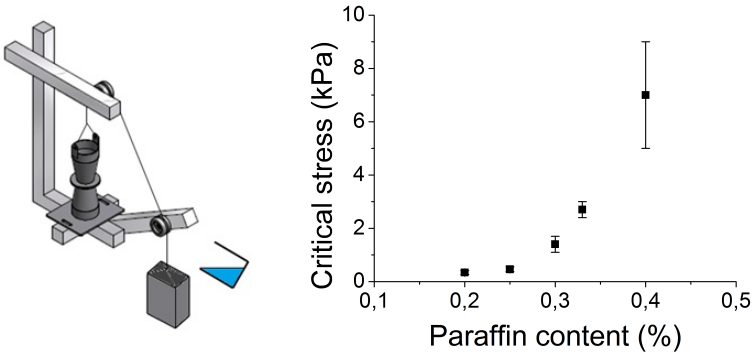

Figure 3: (a) Sketch of the traction test realised on the model soils. (b) Results of the traction test realized on the material $M1$.

fix the strength of the cohesive forces (see Figure 2). This material $M2$ is finally immersed within an erosive liquid, composed of two oils which are non-miscible with the Ucon^{TM} Oil. This oil mixture will be described later in the section 3.2.

3 EXPERIMENTAL SET UP AND PROTOCOL

3.1 *MECHANICAL TESTS*

We carried out mechanical tests to study a possible correlation between erosion parameters and mechanical soil's behaviour. These tests have been realised to measure the mechanical strength of the soil and follow its variation as a function of the bond strength. During the erosion process, the water flow dislodges elementary particles of the soil and carries them away. Afterwards, we studied the tensile strength of the material, to quantify the bond strength and compare it to the resistance against erosion.

At the surface of the soil, a small part of the material pulled off by the fluid during the erosion process. This consistently suggests that the resistance to the separation of the material should be measured.

To this end, a traction test was developed as seen in Figure 3 (a). It is composed of two conical parts assembled at their lower section. The cohesive soil sample is prepared directly inside the system while the lower part remains fixed. Then the upper cone is pulled vertically until failure of the material at the interface between two parts. Figure 3 (b) represents the corresponding tensile strength of the material $M1$ made with sand and paraffin. The tensile strength is obtained from the critical load averaged on several identical tests, for different paraffin content by volume of material.

The tensile strength of this material is between $100Pa$ (approximate accuracy limit of the test) for 0.2% of paraffin and $2640Pa$ for 0.4%. Several measurements have been realised for every paraffin contents, and error bars are obtained from standard deviations.

As expected, the tensile strength increases with the paraffin content, consistently with the assumption that whenever all the particle contacts are bonded, there is a direct relation between the bridge size and the bonding resulting force. This relationship is true only in a specific range of paraffin content, and particularly above a limit content of approximately 0.2% for bead diameter of $3mm$. As a comparison, this limit content enabling capillary bridging at each contact was measured by Fournier et al. (2005), who found a value of 0.07% for glass beads of diameter $375\mu m$ and $555\mu m$ with capillary bridges of water.

3.2 *EROSION TESTS*

3.2.1 *Solid bondings*

Several erosion tests exist to estimate both parameters used in Equation 1. All of these erosion tests consists in an hydrodynamic shear stress applied at the surface of a soil sample to measure the induced erosion rate. For example, Hanson and Cook (2004) measure with the Jet Erosion Test, the variation of a crater depth caused by an impinging jet. Employing the so-called Erosion Function Apparatus, Briaud et al. (2001) measured the thickness variation of a soil's sample regularly lifted upward to ensure a steady position in the flow. Some other researchers, such as Benahmed and Bonelli (2012), used the Hole Erosion Test to measure the enlargement of a hole radius initially drilled through a soil sample, and subjected to pipe flow.

To study soil's resistance against erosion, we use the Jet Erosion Test where a vertical impinging jet strikes the horizontal surface of the soil sample. The test consists in measuring the evolution of the crater depth as the erosion proceeds. With water as erosive fluid, it is possible to calculate the hydrodynamic stress at the interface (Hanson and Cook 2004):

$$\tau = C_f \rho_f U_0^2 \left(\frac{C_d d_0}{h_0 + x} \right)^2 \tag{2}$$

Where the coefficient of friction is $C_f = 0.00416$, the diffusion constant is $C_d = 6.3$, and ρ_f is the fluid density, U_0 the velocity at the jet nozzle, d_0 the nozzle diameter, h_0 the initial distance between the nozzle and the interface and x the crater depth.

The adjustment of the curve which represents the variation of the crater depth as a function of the shear stress, enables to estimate the critical stress ($\tau_c[Pa]$) and the erosion coefficient ($k_d[m^2.s.kg^{-1}]$).

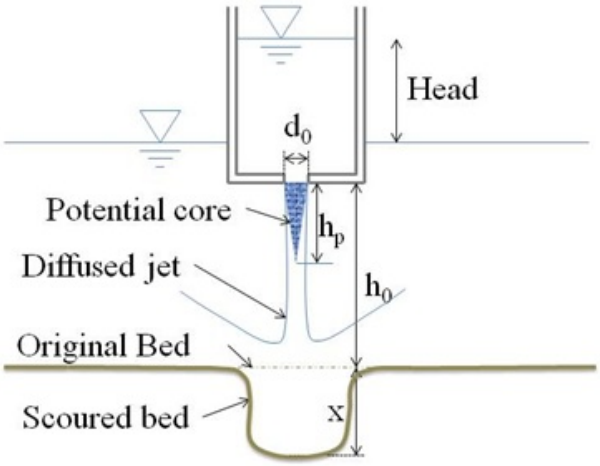

Figure 4: Schema of the Jet Erosion Test (JET)

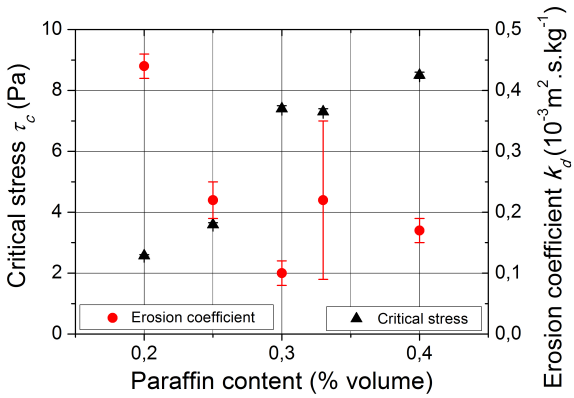

Figure 5: Critical erosion stress and Erosion coefficient as a function of the paraffin content mixed with the Camargue sand (material $M1$).

3.2.2 *Viscous bondings*

As a second step, we adapted the Jet Erosion Test to be able to follow the erosion process of our model soil $M2$. For this purpose, we implemented the techniques already used by Philippe & Badiane (2013), which consist of combining the Refractive Index Matching technique (RIM) with Planar Laser Induced Fluorescence (PLIF). First, the refractive index of the surrounding fluid is matched with the one of the model soil. This erosive fluid is made of two mineral oils, with a mixture viscosity measured to $\mu = 28cP$. A fluorescent dye is added to the liquid, and a planar laser permits the visualization of the material during the erosion process.

The jet velocity is controlled at the nozzle with a gear pump. The jet height h_0 and the nozzle diameter d_0 can be varied. For different configurations, it is thus possible to follow the erosion process in a vertical plane with the planar laser.

The erosive liquid does not allow to calculate the shear stress from Equation 2. Since Equation 2 is specific for the case of water as eroding fluid, we cannot evaluate the erosion parameters. With this kind of setup we can measure an erosion threshold defined when the first beads are dislodged. For this purpose, the jet velocity is increased step by step until the first bead movement. Introducing a stronger and constant flow, we can also measure the final crater depth and the velocity needed to reach this maximum equilibrium depth. Quantifying the jet velocity inside the crater, can provide valuable information on kinetics and erosion threshold. This was realised for beads without cohesion but lies out of the scope of this paper and will be presented elsewhere.

4 RESULTS AND ANALYSIS

4.1 *JET EROSION TEST WITH SOLID BONDINGS*

As explained in previous section 3.2.1, we measured the erosion parameters for material M1 (the sand mixed with paraffin) following the method by Hanson and Cook (2004). A paraffin content of 0.4% could not be exceeded because the crater becomes too narrow to be probed. The evolution of the erosion parameters τ_c and k_d with the paraffin content inside the granular media is shown in Figure 5. As expected, as the paraffin content increases, the material becomes more and more resistant to erosion. Above 0.3% of paraffin this resistance seems to reach a kind of saturation for both τ_c and k_d. Indeed, the critical stress increases from $2.6Pa$ with 0.2% of paraffin to $7.4Pa$ with 0.3%, and $8.5Pa$ with 0.4%, when the erosion coefficient decreases from $4.4\text{x}10^{-4}$ to $10^{-4}m^2s/kg$. The last two values of k_d seem to be a bit higher than expected, and we would need more data to confirm the general trend.

The critical stress can be compared to the critical shear stress for erosion of a non-cohesive medium obtained from the Shields number:

$$Sh_c = \frac{\tau_c}{(\rho_p - \rho_f)gd} \tag{3}$$

Where ρ_p is the particle density and d the particle diameter. From this equation and the data from Andreotti et al. (2011), a value of $\tau_c \simeq 0.2$ is obtained, consistently with an extrapolation of the curve to zero cohesion.

Finally, in spite of important error bars, we can compare these values with the traction tests (Figure 6). It seems that a complex relation holds between the tensile strength of the material and its resistance against erosion. More data are needed to clarify this point.

4.2 *OPTICALLY ADAPTED JET EROSION TEST*

4.2.1 *Cohesive material behaviour*

RIM combined with PLIF enables to follow the erosion process in a vertical plane of symmetry of the jet. Then we can compare the process with cohesionless material and cohesive granular material. Without cohesion, the crater created by the jet in the granular media reaches almost instantaneously a steady depth.

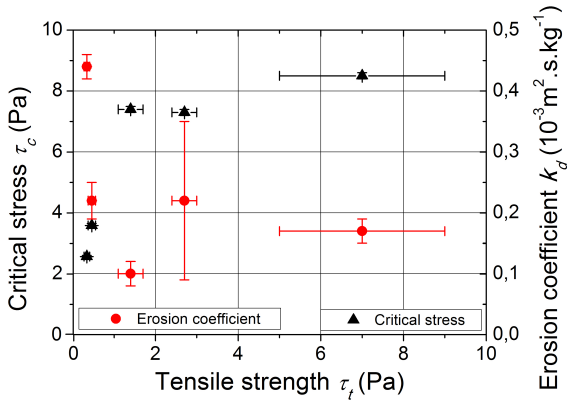

Figure 6: Critical stress (black triangles) and erosion coefficient (red circles) as a function of the tensile strength.

At this depth avalanches continuously fill the crater while beads are evacuated in the same time. A layer of fluidised beads is created around the crater and significant temporal variations of the final depth are observed.

As shown in Figure 7 for the samples with viscous bonds of Carbopol and Ucon^{TM} Oil, the crater reaches a constant depth significantly more slowly. And the more the cohesion is increased, the slower the erosion kinetics become. The final depth seems to follow the same evolution: For the Carbopol, where the tests do not exceed 40 *seconds*, the final depth varies in-between 53 and $31mm$ when the quantity of gel is increased by a factor 6. For the Ucon^{TM} Oil, the tests have been continued until 3000 *seconds*. Final depth varies from $x = 58.2mm$ for 0.2% of Ucon^{TM} Oil to $50mm$ for 1%. However it seems relevant to note that the difference is less than 3 bead diameters when the duration is longer enough. This variation corresponds to the variation of the dynamic final depth without cohesion. Moreover, the variation of the initial distance h_0 is in the same order of magnitude.

However, during the tests we noticed that the viscous bonds could change out of control. In fact, at the very beginning of the test, one happened to be washed out from the model soil without any bead movements. The viscous liquid making the bondings is driven and partially washed out the granular medium by the jet flow. Therefore when the beads begin to be dislodged, there is less bonding matrix inside the material. And during the erosion process, the local quantity of this matrix is always decreasing. Therefore, this effect creates unreliable results because of bond strength cannot be properly controlled in the duration of a test.

4.2.2 *Free jet model*

To obtain more quantitative results about the resistance to erosion, it is crucial to accurately characterise the fluid jet at the surface of the model soils. As previously mentioned, the erosive fluid is an index-matched oil mixture. Its density is slightly smaller than water density, and its viscosity is almost 30 times higher. This gives rise to typical Reynolds numbers

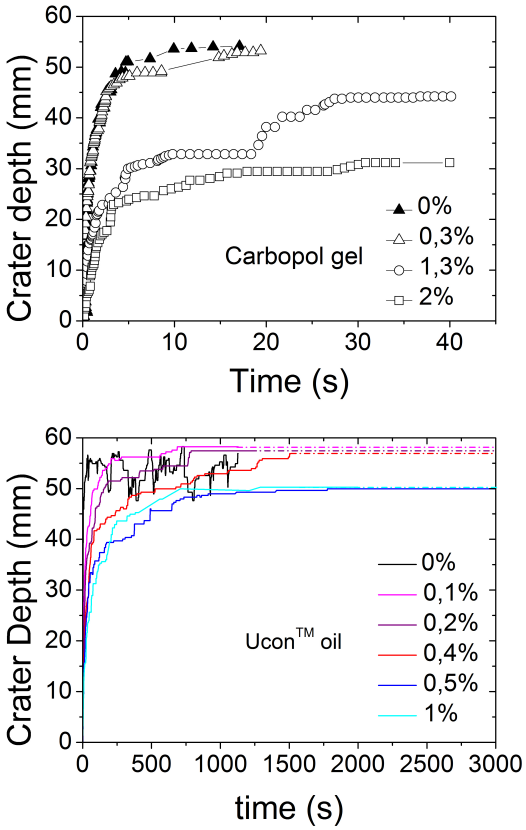

Figure 7: Evolution of the crater depth for model soils made with $3mm$ beads and different quantity of Carbopol gel (up) and Ucon^{TM} Oil (down).

much lower than for usual hydraulic erosion. To study the erosion process inside the material, we need a reliable jet model corresponding to our specific configuration. To this end a study of the jet in the free part (i.e. before interacting with in the material), was carried out with fluorescent tracers spread in the liquid jet to allow fast-camera recording (at $1000fps$ to $1500fps$), and PIV calculation (Figure 8 a.).

The theoretical frame of this study is the auto-similar model of a laminar round jet proposed by Schilchting (1960). This model is based on a virtual jet origin and asymptotic velocity profiles functions

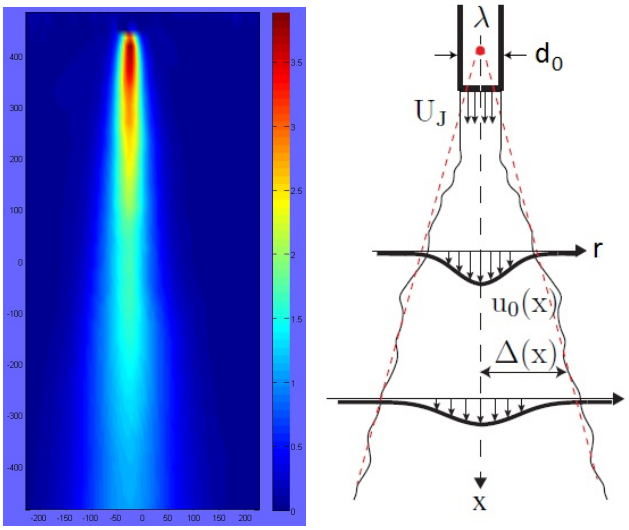

Figure 8: (a) Velocity field of a jet with $U_J = 0.5m/s$ and $h_0 = 5mm$. (b) Sketch of the auto-similar jet model (Badr 2014).

of an auto-similarity variable η (Figure 8 b.):

$$u(x,r) = u_0(x) f(\eta = \frac{r}{\Delta(x)}) \tag{4}$$

Phares et al. (2000) express the decrease of the velocity along the jet centreline $u_0(x)$ and the evolution of the jet diameter $\Delta(x)$. In axisymetrical geometry, these expressions read:

$$u_0(x) = U_J \frac{K_{3DL} d_0}{x + \lambda} \tag{5}$$

$$\Delta(x) = 4\nu \left(\frac{\pi}{3}\frac{\rho}{M}\right)^{1/2} (x + \lambda) \tag{6}$$

With U_J the mean injection velocity, d_0 the nozzle diameter, ρ and ν respectively the density and the viscosity of the fluid, x the distance from the nozzle, λ the distance of the virtual origin to the nozzle. K_{3DL} is a function of $Re_J = \frac{U_J d_0}{\nu}$ and M is the constant momentum flux.

With the velocity field obtained from the PIV calculations, the variables K_{3DL} and λ were adjusted to get a correct estimation of the model for jet Reynolds numbers Re_J between 50 and 200. On Figure 9 we can see the model prediction and the velocity values for different nozzle diameters and jet velocities.

Once empirically adjusted, this model will be used to analyse the behaviour of a cohesive material with solid bondings against such an erosion by a jet, to determine local velocity threshold of erosion, and the erosion kinetics during a test of an index matched cohesive material. The experimental protocol is still being developed and the forthcoming results will be presented later.

5 CONCLUSION AND OUTLOOK

In this work, we presented different methods to analyse the erosion process by a vertical round jet impinging model soils. The first method consists in comparing mechanical tests and erosion tests on a granular material with solid bondings made of paraffin. The results show a qualitative correlation between the tensile strength of the sample, and its erosion parameters evaluated with the Jet Erosion Test.

The second method was developed to analyse the erosion process with two combined visualization techniques (RIM and PLIF). These techniques require the use of refractive index matching bondings to create transparent bridges between the grains. The monitoring of the process enables to have a qualitative idea of the impact of cohesion on erosion, no quantitative results can be obtained for viscous bondings which cannot be properly controlled during an erosion test.

The perspectives for a future work are to find a solid material capable to keep material transparency and follow the erosion processes.

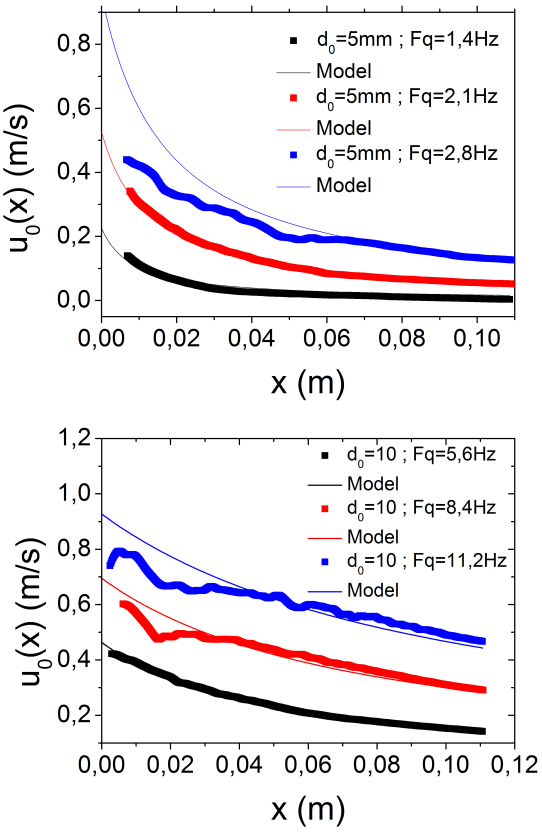

Figure 9: Maximum velocity in the jet centreline and fitted model for nozzles of $5mm$ and $Re_J = 42$; 63 and 85 (up) and for nozzles of $10mm$ and $RE_J = 85$; 130 and 170(down). For fastest velocities the frame rate and the PIV calculation was probably less adapted to the real velocities.

REFERENCES

Andreotti, B., Y. Forterre, & O. Pouliquen (2011). *Granular Media: Between Fluid and Solid*. Paris: EDP Sciences CNRS Editions.

Ariathurai, R. & K. Arulanandan (1978). Erosion rate of cohesive soil. *J. Hydraul. Division ASCE 104(2)*, 279–283.

Badr, S., G. Gauthier, & P. Gondret (2014). Erosion threshold of a liquid immersed granular bed by an impinging plane liquid jet. *Physics of Fluids 26*, 023302.

Béguin, R., P. Philippe, & Y.-H. Faure (2013). Pore-scale flow measurments at the interface between a sandy layer and a model porous medium: Application to statistical modeling of contact erosion. *J. Hydraul. Eng. ASCE 139(1)*, 1–11.

Benahmed, N. & S. Bonelli (2012). Investigating concentrated leak erosion behaviour of cohesive soils by performing hole erosion tests. *European Journal of Environmental and Civil Engineering 16(1)*, 43–58.

Briaud, J. L., F. C. K. Ting, H. C. Chen, Y. Cao, W. Han, & K. W. Kwak (2001). Erosion function apparatus for scour rate predictions. *J. Geotech. Geoenviron. Eng. 127*, 105–113.

Dufois, F., R. Verney, P. LeHir, & F. Dumas (2014). Impact of winter storms on sediment erosion in the rhon river prodelta and fate of sediment in the gulf of lions (north western mediterranean sea). *Continental Shelf Research 72*, 57–72.

Foster, M., R. Fell, & M. Spannagle (2000). The statistics of embankment dam failures and accidents. *Can. Geotech. J. 37*, 1000–1024.

Fournier, Z., D. Geromichalos, S. Hermingaus, M. M. Kohonen, F. Mugele, M. Scheel, M. Schulz, C. Schier, R. Seemann, & A. Skudelny (2005). Mechanical properties of wet granular materials. *J. Phys.: Condens. Matter 17*, S477–S502.

Hanson, G. J. & K. R. Cook (2004). Apparatus, test procedures, and analytical methods to measure soil erodibility in situ. *Applied Engineering in Agriculture 20(4)*, 455–462.

Luu, L. H., P. Philippe, & G. Chambon (2015). Experimental study of the solid-liquid interface in a yield-stress fluid flow upstream of a step. *Physical Review E 91*, 013013.

Parchure, T. M. & A. J. Mehta (1985). Erosion of soft cohesive sediment deposits. *J. Hydraul. Eng. ASCE 111*, 1308–1326.

Parteniades, E. (1965). Erosion and deposition of cohesif soil. *J. Hydraul. Division ASCE 91*, 105–139.

Phares, D. J., G. T. Smedley, & R. C. Flagan (2000). The wall shear stress produced by the normal impingement of a jet on a flat surface. *J. Fluid Mech. 418*, 351–375.

Philippe, P. & M. Badiane (2013). Localized fluidization in a granular medium. *Physical Review E 87*, 042206.

Schilchting, H. (1960). *Boundary layer theory*. New York: McGraw Hill Book Co.

VanProoijen, B. C. & J. C. Winterwerp (2010). A stochastic formulation for erosion of cohesive sediments. *J. Geophys. Res. 115*, C01005.

VanRijn, L. C. (1984). Sediment pick-up functions. *J. Hydraul. Eng. 110*, 1494–1502.